Experimental Evaluation of the Dynamic Route Map in the Reset Transition of Memristive ReRAMs

David Maldonado[a], Mireia B. Gonzalez[b], Francesca Campabadal[b], Francisco Jiménez-Molinos[a], M. Moner Al Chawa[c], Stavros G. Stavrinides[d], Juan B. Roldan[a], Ronald Tetzlaff[c], Rodrigo Picos[e], Leon O. Chua[f]

[a]*Dept. de Electrónica y Tecnología de Computadores, Universidad de Granada, Spain*
[b]*Institut de Microelectrònica de Barcelona, IMB-CNM, CSIC, Barcelona, Spain*
[c]*Institute of Circuits and Systems, Technische Universität Dresden, Dresden, Germany*
[d]*School of Science and Technology, International Hellenic University, Thessaloniki, Greece.*
[e]*Physics Department, University of Balearic Islands, Balearic Islands, Spain.*
[f]*Electrical Engineering and Computer Science Department, University of California, Berkeley, CA, USA*

Abstract

In this paper, we analyze the reset transition in bipolar TiN/Ti/HfO_2 (10 nm)/Al_2O_3(2 nm)/W ReRAM devices using a tool that allows studying the temporal behaviour of these devices. This tool, the Dynamic Route Map (DRM), provides information about the temporal evolution of the state variable that governs the behaviour of the device, thus allowing an increased insight into resistive switching processes.

Here, we show that this DRM is a powerful tool, that may help explaining some non intuitive behaviours of memristors, like the difference in the reset voltage when the inputs are from different frequency or shape. Using this tool, this fact can be explained as a different trajectory on a unique surface defining the device.

As a first step, we have used two different models, one based on a physical description, and another one based on the mathematical definition of memristor as a non linear relation between charge and flux. We check that similar DRM can be obtained from both models.

Additionally, several series of set-reset transitions have been measured using voltage ramps of different slopes. From the measured transitions, the corresponding resistance has been extracted and, assuming conductive filaments (CF) as the switching mechanism, the corresponding CF radius has been calculated. Using these data, we show that explanations from the model are also supported when using experimental data, thus proving the validity of the approach.

1. Introduction

The apparent symmetry between the relations of the four fundamental electrical magnitudes, namely the current i, the voltage v, the charge q and the flux φ, was something that passed unnoticed for many years in circuit theory.

Email addresses: s.stavrinides@ihu.edu.gr (Stavros G. Stavrinides), rodrigo.picos@uib.es (Rodrigo Picos)

It was this idea that led Leon O. Chua, during the early 70s, to present the axiomatic introduction and the related description of a fourth (missing at that moment) electrical element, named the Memristor [1]. Its name originated from the fact that such an element should behave as a resistor endowed with memory, these two properties (resistance and the feature memory) being unified in one element. In fact, memristors had been described many years ago [2], though they had never been in the mainstream of electrical or circuit theory. Besides, Chua's work led to the generalization of a class of devices as well as systems that are inherently nonlinear and governed by a state-dependent, algebraic relation accompanied by a set of differential equations, which are called memristive systems or devices [3].

As a result of the inherent memory feature embodied in memristors, these novel devices are expected to be one of the key enablers of a technological breakthrough in integrated circuit (IC) performance-growth, beyond and more than Moore [4]. Among others, they are expected to provide a solution to the classical problem of the bottleneck in data transmission between memories and processors. The Internet-of-Things (IoT) and other edge computing applications are expected to be areas where the introduction of memristors and memristive devices would be beneficial, or even a radical changer of the related technological landscape. Thus, an increasing number of memristor-based applications has already been proposed: new kind of memories (ReRAMs, MRAM, etc.) [5, 6, 7], innovative new sensor devices [8, 9], or fundamental elements in bio-inspired systems (artificial neural networks (ANNs) and other) [10], among many others.

On the other hand, memristive devices can be nowadays implemented in a wide range of technologies, from spintronics [11] to organic materials [12, 13] and many different oxides [14, 15, 16, 17], or even emulators [18, 19, 20, 21]. However, and up to the best of our knowledge, very few foundries are including memristors in their design repertoire, as it customarily happens with other passive elements, like resistors or capacitors. This is due to the inadequate level of maturity of all the up-to-date proposed memristive technologies, which is a drawback that is expected to be solved in the near future.

Simulating a new design incorporating memristors is not a straightforward task; many good models have been proposed, both using the classical approach that utilizes current and voltage [22, 23, 24, 25, 26], or the more recent charge and flux approach [27, 28, 29, 30], which historically had been also used in oxide breakdown. However, most of these models appear to have drawbacks that make the simulation of large circuits rather difficult or even impractical [31]. Besides, some of the main problems of current memristor device technologies are: the variability they exhibit, from cycle to cycle [32, 33]; and the short number of cycles they can withstand (between 10^6 and 10^8 cycles).

A very good test to show the goodness of a model is the so-called Dynamic Route Map (DRM), that plots the evolution of the governing variable of a system in front of its rate of change (i.e., its temporal derivative). As will be explained later, this representation is a powerful tool that may provide significant insight into the inner workings of the device. In this work, we aim to show experimentally that the DRM tool actually makes sense in memristive ReRAMs, and can be used as a unifying tool to describe the different behaviour of the devices under various stimuli. We will show that this behaviour can be described as a different trajectory on the same surface. Specifically, we will focus on the Low Resistance to High Resistance State (LRS to HRS, or RESET) transition, since

it is considered to be more complex than the SET transition and, thus, a more appropriate example to highlight the merits of the DRM technique.

The paper is structured following this idea: after this introduction, Section 2 introduces the basic principles of formal memristor modelling, where the DRM naturally appears. Then, Section 3 is devoted to introduce the concept of the Dynamic Route Map and its applications, as well as two different models showing two different approaches to DRM. The first model directly introduces an equation for the variable of concern (the radius of a conductive filament), while the second model derives the effective radius from the calculation of the conductance. Section 4 presents the results obtained by applying different waveforms to a single device, showing that we can obtain experimentally its DRM. Finally, Section 5 ends the paper summarizing the main points and results.

2. Memristor Modelling Framework

A fundamental theoretical framework for studying memristors and circuits presenting memristive behaviour in the flux–charge (φ-q) domain, was developed by Corinto *et al.* in [34]. In that paper, the authors explain the advantages of using the flux–charge (φ-q) domain in studying memristor elements, compared to the current–voltage (i-v) domain.

On the other hand, utilizing the taxonomy proposed in [35], memristors are classified according to their proximity to the original definition of the memristor. Thus, three main categories of memristor devices emerge, namely the ideal, the generic, and the extended memristor. In the same work [34], the essential mathematical framework describing their behaviour was also developed. This extended categorization emerged as a necessity in order to include theoretically the description of pinched, hysteretic behaviours demonstrated by various elements, not only in circuit theory and electronics but also in nature.

Among the different categories presented above, the class of extended memristors is the most general one and it refers to memristors that have extra state variables (next to φ and q). For the specific case of flux-controlled memristors, they are described by Eqs. (1) to (3):

$$i = G(\varphi, v, \mathbf{x}) \cdot v \tag{1}$$

$$\dot{\mathbf{x}} = \mathbf{g}_{\varphi}(\varphi, v, \mathbf{x}) \tag{2}$$

$$\dot{\varphi} = v \tag{3}$$

The nonlinear memconductance G in Eq. (1) represents the inverse memristance M of an extended memristor, while v is the voltage applied to the memristor, and φ is the flux or voltage first momentum. The vector $\mathbf{x}$ stands for a *set* of extra state variables, which includes physical magnitudes according to the memristive system; indicatively they could be the internal temperature, the radius of a conducting filament, or any other non-electrical variable describing the state of the memristor. In addition, the dynamics of the state variables $\mathbf{x}$ are governed by g_{φ} and Eq. 2. It is noted that all the real-world memristor devices that have appeared until now, are indeed extended memristors.

Taking into account the Lagrangian L and the Jacobian $\mathbf{J}$, these are defined in Eqs. (4) and (5), respectively.

$$L(\varphi, v, \mathbf{x}) = \frac{\partial g_{\varphi}(\varphi, v, \mathbf{x})}{\partial v} \tag{4}$$

$$\mathbf{J}(\varphi, v, \mathbf{x}) = \left(\frac{\partial g_{\varphi}(\varphi, v, \mathbf{x})}{\partial x_1}, ..., \frac{\partial g_{\varphi}(\varphi, v, \mathbf{x})}{\partial x_n} \right) \tag{5}$$

If no parasitic effects are present, then extended memristors can be simplified to generic memristors (or, simply, memristors). That is because function g_{φ} is only dependent on flux φ and the state variables $\mathbf{x}$, thus $L = 0$. Finally, ideal memristors (those corresponding to the original definition described by [1]) are generic memristors that demonstrate no other state variable dependence, thus, $J = 0$.

A special case of Eq. (2) is often referred to as the power–off plot (POP) equation and determines the memory capability of the system under no excitation; in this case for $v = 0$ or $\varphi = constant$. It is apparent that if the POP equation is zero, the system presents a long–term memory since the state variable will not change with time, while if it is different than zero, the system is capable of exhibiting only short–term memory.

It is noted that the above framework has been already used in successfully modelling different kinds of memristive systems, further improving the generalized framework for compact modelling in the flux-charge space [36]. Other relevant works using this approach could also be found, like in the case of [37] where a charge-dependent mobility model was used to describe a memristor, [28] or [30] which presented semi-empirical models for ReRAMs as memristors, [38] that described a Monte Carlo model for ReRAMs, [39] which derives a delay model for memristor–based memories utilizing a flux-charge description, or [27] where a model for phase change memories is presented. Finally, two examples of experimental characterization of a memristive system utilizing the flux-charge notation, are presented in [40], where a light bulb is determined to be a generic memristor and in [41, 42], where the influence of waveform frequency and shape are discussed.

3. The Dynamic Route Map

3.1. The Dynamic Route Map Technique

Phase space, initially introduced by J. Liouville [43], is a space proposed by Poincaré [44] for studying nonlinear systems. The study of nonlinear systems in phase (or state) space is an established approach in nonlinear dynamics, since important attributes of the systems clearly emerge within. The case of a two dimensional phase space, that of the phase plane, i.e. the space of X vs. dX/dt (where X is a state variable of the studied system), was introduced and utilized by the Ehrenfests in the early 1900s [45].

As already mentioned above, memristors are described, in general, by Eqs. (1) - (3). These equations refer to the case of extended, flux-controlled memristors; while a duality principle holds for the case of charge-controlled ones. Considering their hysteretic behaviour (fingerprint) and furthermore their switching

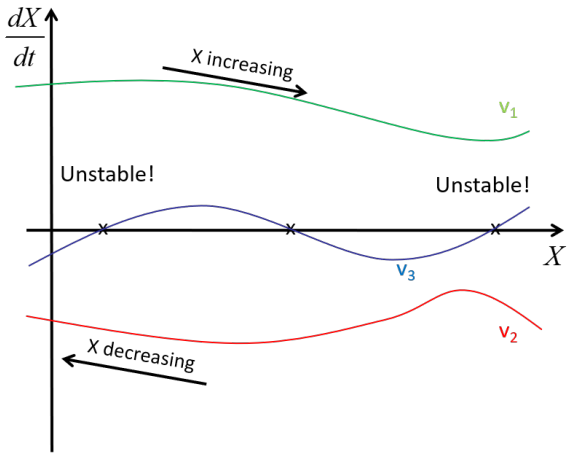

Figure 1: A typical DRM for an arbitrary system, having as a parameter the voltage applied. It includes three distinct cases; the case in middle provides an example of identifying the equilibrium points of a system - two unstable (labeled x) and a stable one (unlabelled x), in this case.

properties, memristors clearly emerge as nonlinear elements [46]. Thus, it is expected that studying their properties within a phase space, would provide useful information about the devices and their dynamical properties.

To this direction, the Dynamic Route Map technique, a method mounted within the phase plane, was proposed to be applied in the case of memristors; thus providing information on specific features they demonstrate, such as their switching properties [47].

Beginning from the definition in the case of memristors, the Dynamic Route defines the course of a non-zero state variable, within its phase plane, when memristor's voltage (for flux-controlled) or current (for charged-controlled) gets a specific value. Notice that this is equivalent to plot Eq. 2. Consequently, the DRM is a parametric collection of a theoretically infinite number of Dynamic Routes [47]. In Fig. 1, a typical example of a DRM is presented. In this figure three distinct cases appear; the most characteristic is the case in middle, which includes a stable and two unstable equilibrium points (where $dX/dt = 0$).

Important features of DRM and consequences coming out of it, include the following (for a comprehensive and detailed presentation, see [47]):

- DRM is infinitely dense.
- For visualizing DRM, only some of the Dynamic Routes (a finite number) are displayed.
- Any point of a dynamic route, belonging to the upper half plane, moves to the right (increasing the value of the variable).
- For a dynamic route belonging to the upper half plane, the higher it stands, the faster its points move along their tracks (to the right).
- Any point of a dynamic route, belonging to the lower half plane, moves to the left (decreasing the value of the variable).

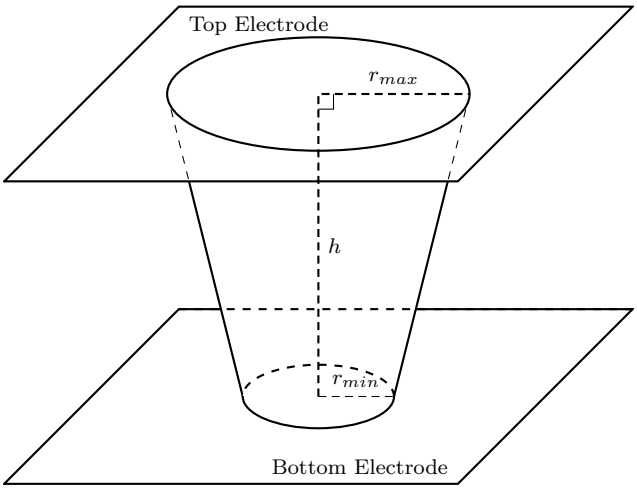

Figure 2: Parameters of a conductive filament when considered as a truncated cone.

- For a dynamic route belonging to the lower half plane, the lower it stands, the faster its points move along their tracks (to the left).
- Points laying on the horizontal axis, are equilibrium points (since their possess null velocity $dX/dt = 0$).
- An equilibrium point in 2D may be stable (the trajectories are such that the points converge towards it) or unstable (the points diverge from it).

The dynamic route for a zero parameter value – in the case of memristor for zero voltage v=0 (or current i=0) – reduces to the Power-Off Plot (POP). The POP has been proposed as a tool for identifying memristor volatility in simple visual way. According to [47], any memristor demonstrating one stable and two unstable equilibrium points appears to be a volatile device; on the contrary, non-volatile memristors demonstrate one unstable and two stable equilibrium points.

Finally, it is worth commenting on one important issue that could be easily identified by utilizing the DRM: the dynamics demanded in order to achieve switching in a memristor device (i.e. setting and resetting it) can be visualized on the DRM. This way it becomes clear that these two operations could be achieved by obliging the operation point to change the dynamic route for a specific period of time. This operation is usually achieved by the application of suitable positive or negative pulses that compel switching between two equilibrium points.

3.2. Example of DRM: Toy Model

For the shake of clarity, a simple toy model, that can be easily conceived, is presented in this section. Let's consider that the memristive behaviour is mediated by a conductive filament, defined as in Fig. 2. To provide a physical basis, we can consider a model described by [48], but strongly simplified to retain only some features. We can describe this model using the formalism presented in the previous section as the following set of equations:

$$i = G(\varphi, v, r) \cdot v \tag{6}$$

$$\dot{r} = g_{\varphi}(\varphi, v, r) = A \cdot v \cdot exp(-\frac{B \cdot r^2}{a + v}) \tag{7}$$

$$G(\varphi, v, r) = K\frac{r^2}{h} \tag{8}$$

$$L(\varphi, v, \mathbf{x}) = \frac{\partial g_{\varphi}(\varphi, v, \mathbf{x})}{\partial v}$$
$$= A \cdot e^{-\frac{Br^2}{a+x}} \frac{a^2 + 2av + v(Br^2 + v)}{(a + v)^2} \tag{9}$$

$$\mathbf{J}(\varphi, v, \mathbf{x}) = \frac{\partial g_{\varphi}(\varphi, v, \mathbf{x})}{\partial r}$$
$$= -2\ A\ B\frac{v\ r}{a + v} \cdot exp(-\frac{B \cdot r^2}{a + v}) \tag{10}$$

In the equations above A, B, and K are constants related to the technology, and h is the device dielectric thickness. The radius r is defined as an effective average between r_{max} and r_{min} in Fig. 2. This model corresponds to an extended memristor device, since neither the Laplacian (Eq. 9) nor the Jacobian (Eq. 10) are nil. In addition, we can see that the POP equation (Eq. 7 for $v = 0$: $\dot{r}(v = 0) = 0$) is nil. Thus, the model corresponds to an extended memristor with long-term memory.

This very simple model already leads to a behaviour showing some of the most intriguing dynamics of real resistive memristor devices, namely a high dependence on initial conditions (i.e., the initial radius of the CF), and a reset voltage (i.e., the voltage where the radius gets to zero) depending on both the initial conditions and on the shape and frequency of the used waveform, as has been shown experimentally [41, 49].

The dependence on the input signal shape and frequency of this model is shown in Fig. 3, where four different signals are plotted versus time until the filament breaks at $r = 0$, all starting from the same initial point. Notice that this is equivalent to the reset point. The same waveforms are plotted in Fig 4, but plotting the current versus the voltage. In the case of the sinusoidal waveforms (blue and black lines), the memory effect is clearly shown in the apparition of lobes. Thus, this demonstrates that a repetitive signal can be used to set the desired resistance of the device.

On a separate thread, we have then used Eq. 7 to plot the evolution of the radius versus the radius (the Dynamic Route Map, DRM), in Fig. 5. In this plot, it is clearly seen that the radius decreases faster for higher voltages and smaller radius, as expected.

Finally, we have used the same Eq. 2 to plot a 3D surface in Fig. 6, where we have also plotted the evolution of the waveforms in Fig. 3. Notice that when using this representation, the evolution of the system means that all the waveforms simply move over the surface defined by Eq. 7, thus providing a valuable insight into the dynamics that govern the device.

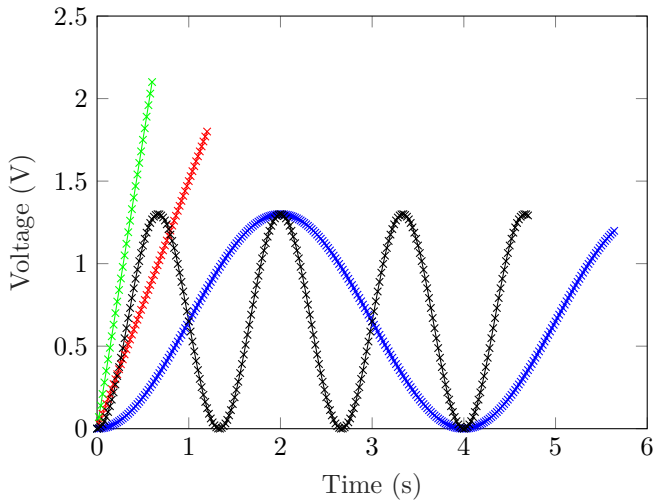

Figure 3: Temporal evolution of the curve of the applied signal until the reset point for different waveforms. Notice that the curves stop when the reset point is reached (the CF radius gets to zero) and, thus, have different lengths.

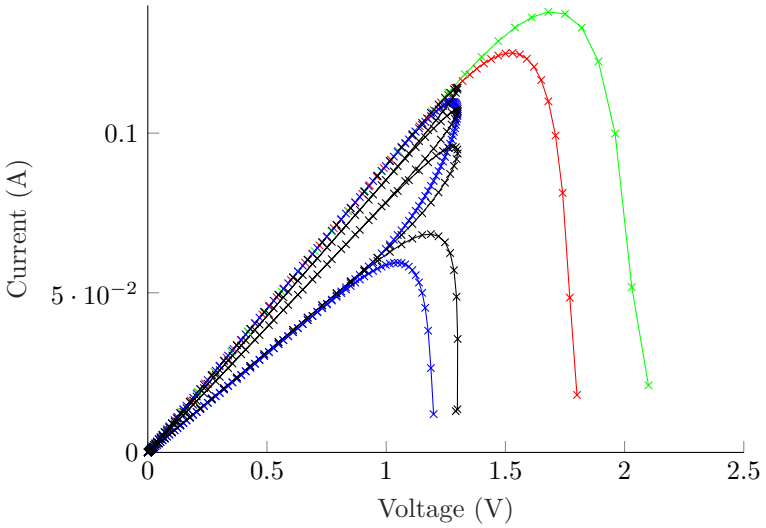

Figure 4: Current vs Voltage evolution of the curve of the applied signal until the reset point for different input waveforms, as shown in Fig. 3. Notice that the curves stop when the reset point is reached (the CF radius gets to zero).

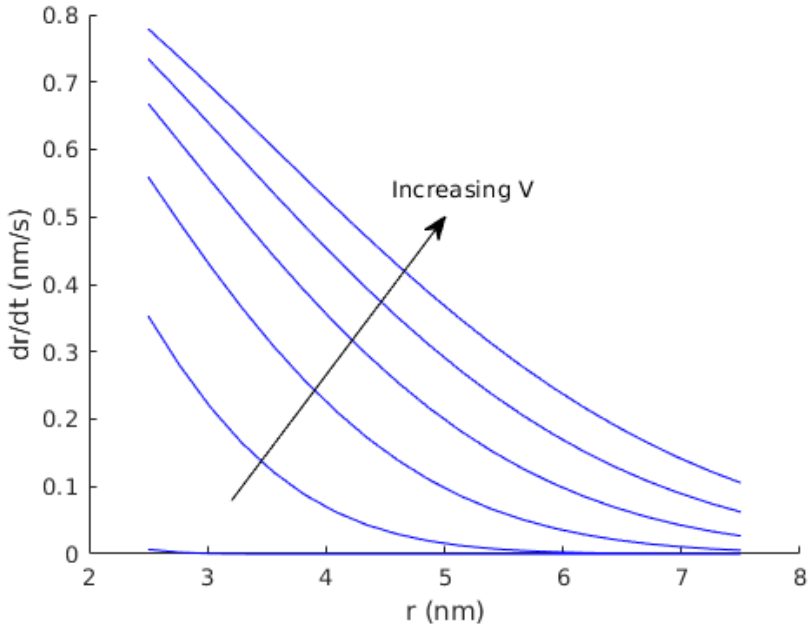

Figure 5: DRM of the CF radius, as in Eq. 7, for various constant voltages. The arrow shows the direction of increasing voltage between 0 and 2V, with 0.4V increment.

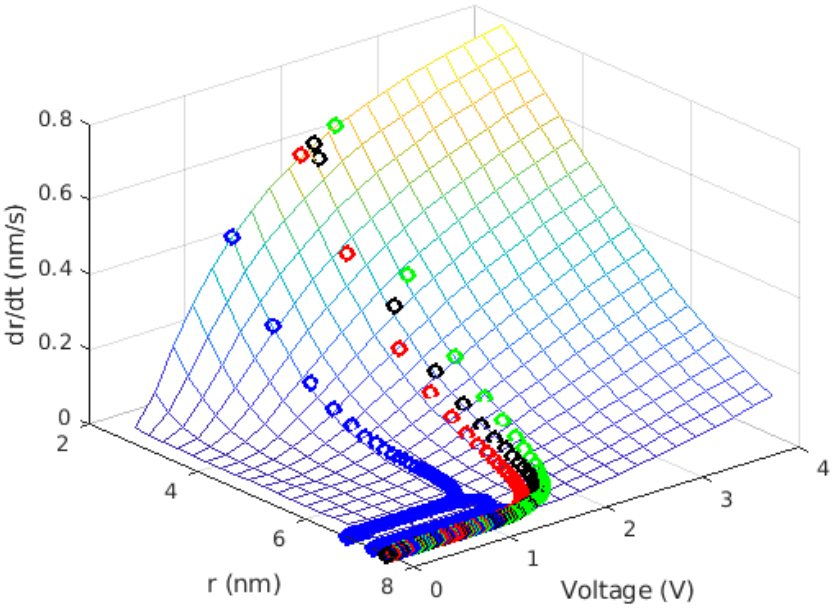

Figure 6: Evolution of the curve of the applied signal in the DRM space. The curves are extracted from those in Figures 4 and 5, as calculated with Eqs. 6-10. Notice that the curves stop when the reset point is reached, which is when the CF radius gets to zero. The surface corresponds to the 3D representation of Fig. 5.

3.3. DRM in a Flux-Charge model

As another example, we will consider an already existing model [50, 51, 52, 53], derived from that presented in [28]. This model starts by defining a relation between charge and flux, as in Eq. 11.

$$Q = Q_0 \cdot (\frac{\phi}{\phi_0})^n \tag{11}$$

The memconductance G is then described by:

$$G = \frac{dQ}{d\phi} = n \cdot \frac{Q}{\phi} \tag{12}$$

Its rate of change can be written by taking the derivative of the memconductance (12) as following:

$$\frac{dG}{dt} = G \cdot v \cdot \frac{n-1}{\phi} \tag{13}$$

Notice that this is already the DRM equation for the conductance. However, it can written in a more compact way assuming that n is nearly a constant:

$$\frac{dG}{dt} = G\ (n-1)\ \frac{d}{dt} ln(\phi) = G\ \frac{d}{dt} ln(\phi^{n-1}) \tag{14}$$

The effective radius r_{eff} of the conductive filament can also be calculated easily, assuming a cylinder [30, 38]:

$$G = \frac{\sigma\ \pi\ r_{eff}^2}{h} \tag{15}$$

where σ is the conductance of the conductive filament, assumed to be nearly constant.

Then, the radius and its rate of change can be expressed as:

$$r_{eff} = r_0 \sqrt{G} \tag{16}$$

where $r_0 = \sqrt{h/\sigma\pi}$.

$$\frac{dr_{eff}}{dt} = \frac{r_0}{2\sqrt{G}} \frac{dG}{dt} = \frac{1}{2} r_{eff}\ \frac{d}{dt} ln(\phi^{n-1}) \tag{17}$$

For instance, let us consider the case of a simple ramp for the input voltage with slope α:

$$V = \alpha t \tag{18}$$

Then the flux is:

$$\phi = \frac{1}{2}\alpha t^2 + \phi_0 \tag{19}$$

Then, the DRM can be expressed as:

$$\frac{dG}{dt} = (n-1)\ G\ \frac{d}{dt} ln\left[\left(\frac{1}{2}\alpha t^2 + \phi_0\right)\right] = \frac{(n-1)\ G\ \alpha t}{\frac{1}{2}\alpha t^2 + \phi_0} \tag{20}$$

or using the effective radius:

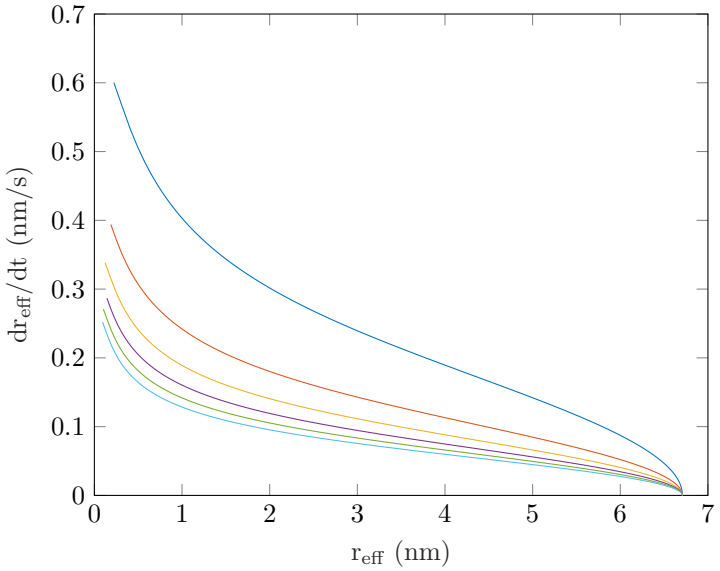

Figure 7: DRM for the effective radius and its temporal derivative for different voltage ramp slopes (α), using memristor model described by Eq. 21. Notice that dr_{eff}/dt is plotted in absolute value.

$$\frac{dr_{eff}}{dt} = \frac{(n-1)\ r_{eff}\ \alpha t}{\alpha t^2 + 2\phi_0} \tag{21}$$

Figure 7 plots Eq. 21 for different values of the slope α to obtain the DRM in the case of the effective radius. It can be seen that the rate of change of the radius r_{eff} increases when the radius decreases, which is coherent with a thermal model where the relation between the volume where the power is generated and the surface where the power is dissipated goes as $1/r_{eff}$. This behaviour implies a higher power dissipation efficiency for smaller radius, thus causing higher radius decreasing rates due to higher temperatures.

4. Experimental Measurements and Results

After introducing the DRM technique, we have presented two different examples on how to calculate it in the case of two models. These two examples have shown how to interpret the evolution of the system under different input waveforms. This method has then been utilized to interpret data obtained from real devices.

We have measured TiN/Ti/HfO_2(10 nm)/Al_2O_3(2 nm)/W devices, where the dielectric layers were grown by Atomic Layer Deposition. For all our measurements, the W layer was grounded and the different input voltage signals were applied to the TiN/Ti top electrode. To estimate the DRM, we considered the effects of different ramp speeds and sine function voltage signals of different frequency, measuring 100 Resistive Switching (RS) cycles for each different waveform as in [49]. The ramp speeds were (0.08, 0.16, 0.24, 0.34, 0.43) V/s, while the sinusoidal signal frequency were (0.0131, 0.0340, 0.0540) Hz.

The measurements were performed by using a HP 4145B parameter analyzer and a probe station. The signals were generated by the 4145B, which was GPIB connected and controlled remotely. This same instrument was also measuring the currents through the devices under test. Figure 8 shows some examples of the I-V curves measured for a selected device under the different inputs waveforms, where a significant dependence on frequency and shape is observed, as expected [41, 49].

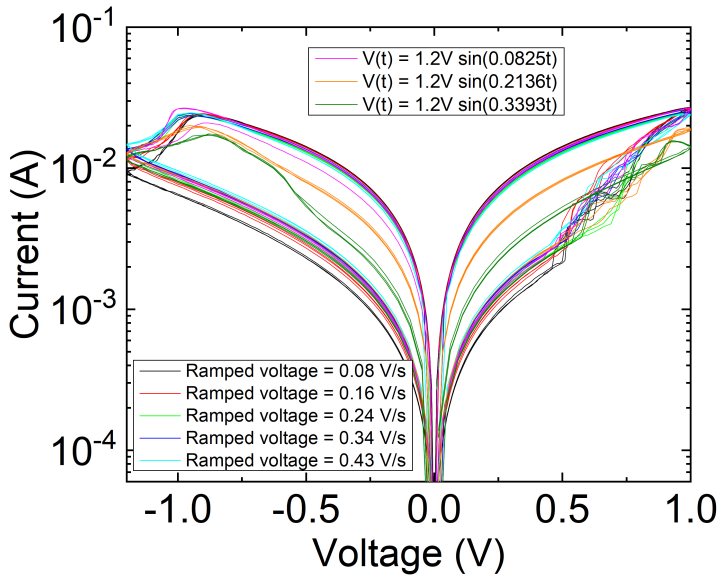

Figure 8: Examples of different I-V curves of the selected devices under different waveform excitation.

This work has focused on the low (LRS) to high resistance state (HRS) transition. In our case, for slow signals, and assuming that the conductive filament (CF) has a truncated-cone shape, we could consider the minor radius r of the CF as the sole estate variable, as in Fig. 2 (in the most common case of filamentary conduction ReRAMs).

For this region, the resistance R of the conductive filament (CF) was estimated by using Eq. 22 and the values in Table 1. The CF shape was assumed to correspond to a truncated-cone with small radius r, high radius $4 * r$, and thickness h. Using these assumptions, we have estimated the radius evolution for each measured curve during the LRS to HRS. This process is depicted in Fig. 9, and can be divided into three parts:

1. **IV curves**. The I-V curves were measured for each LRS to HRS transition, and the reset point was determined.
2. **Resistance Determination.** From the previous experimental curves, the resistance up to the reset point was calculated using Ohm's Law.
3. **Radius calculation.** Using the resistance calculated in the previous step, and the value of the conductance in Table 1, the value of the radius was estimated as:

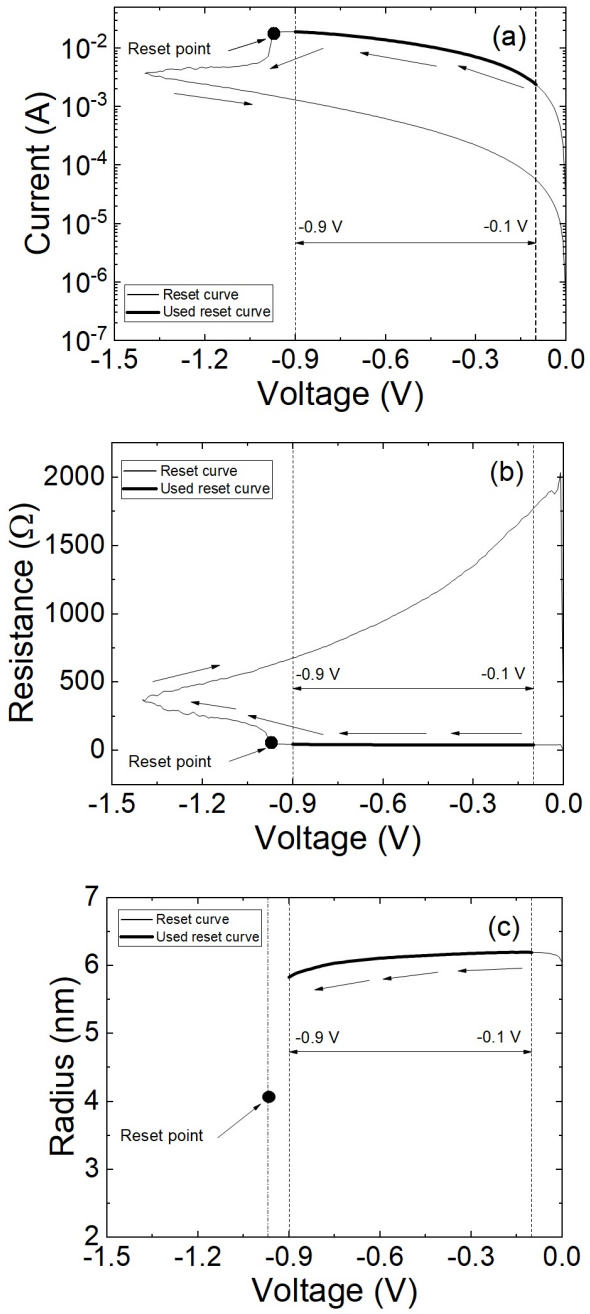

Figure 9: a) Current versus applied voltage (the reset curve section employed in the calculation is shown in bold) obtained making use of an input voltage with a ramp of -0.08 V/s; b) The resistance is extracted and shown versus the applied voltage; c) The conductive filament radius versus applied voltage is estimated.

Table 1: Technological parameters and fitting constants used for the TiN/Ti/HfO_2/Al_2O_3/W stack used to fabricate the ReRAM memristive device. (* The value of h is calculated by adding the thicknesses of the HfO_2 layer (10 nm) and theAl_2O_3 (2 nm)).

Parameter	**Value**	**Units**
h $(*)$	12	nm
σ	$5{\cdot}10^5$	S/m

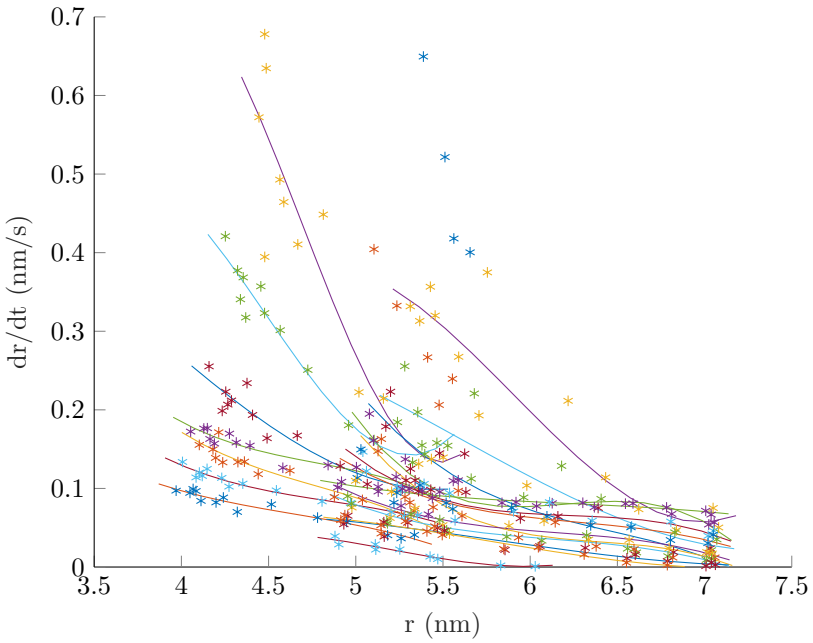

Figure 10: Radius of the conductive filament versus dr/dt (in absolute value), extracted from experimental measurements as described in the text. The points correspond to the evolution of the CF, as estimated, and the lines show their moving average.

$$r = \sqrt{\frac{h}{4\pi R\sigma}} \tag{22}$$

Since the thermal inertia can be neglected in the low frequency operation regime considered for our calculations, a first order memristor can be assumed. Plotting the values of radii extracted, using Eq. 22, for several reset curves, applying both ramp input voltage signals and sinusoidal input waveforms $v(t)$, results in Figure 10. To create this figure, we first have plotted all the [r, dr, v(t)] points. Then, to obtain a drawing similar to Figure 5, we plot in Fig. 10 the points corresponding to constant V values. In this same Figure, the lines correspond to a moving average. It has to be pointed out that each full I-V cycle causes different initial CF r values. Notice that the moving averages strongly resemble those in Figures 6 and 7, as expected.

As a second step, we have plotted in a 3D graph the [v, r, $abs(dr/dt)$] triplets, corresponding to the experimental measurements (see Figure 11) to further emphasize that their dynamic behaviour is located on a surface. These

points define the DRM surface, where all the trajectories of the system must lay on. It is apparent in this Figure that the DRM behaviour seems to hold true for all the curves considered. The deviations from this surface are attributed to random fluctuations in the initial size and shape of the conductive filaments, which are created anew in the set part of the cycle. Additionally, another source of error is the propagation of the measurement error and noise, which directly translates into deviations of the estimated CF radius.

It is worth pointing out the existence of two secondary bumps in Fig. 11, probably due to multiple CF. These bumps are clearly exposed in Fig. 12, which is simply a rotation of Fig. 11.

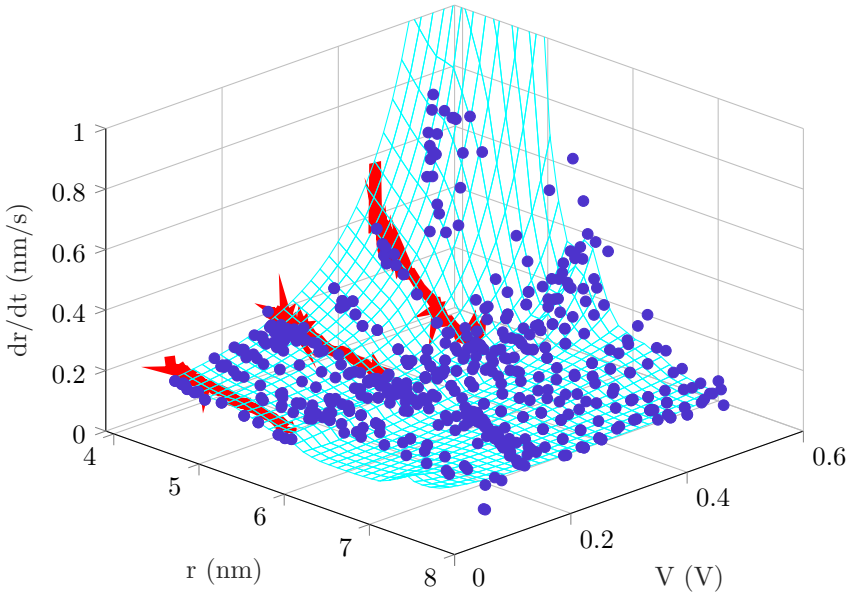

Figure 11: 3D plot of the experimental DRM, showing also an empirical surface fit. The points correspond to a random selection of extracted [V, r, dr/dt] triplets. For the sake of clarity, three specific indicative trajectories are marked as red lines.

It has to be noted that results from both the toy model (Eq. 7) and the charge and flux model (Eq. 21), closely resemble experimental data; thus showing that the model reproduces the physics behind the reset mechanism, in a reliable way. Specifically, all of them show very similar behaviour in the evolution of the radius time derivative, which accelerates as the radius tends to zero; further reflecting the positive feedback process between conductance and temperature, which is behind reset events in resistive switching devices.

Moreover, it has to be noted that the evolution of the experimental curves dr/dt vs. r and $v(t)$ fall on a surface in the 3D plot, as predicted by the models, and as shown in Figure 11. This last result hints for the fact that the response of the device under an arbitrary input is being mainly governed by the initial conditions (aka the initial CF radius) and the shape of the DRM.

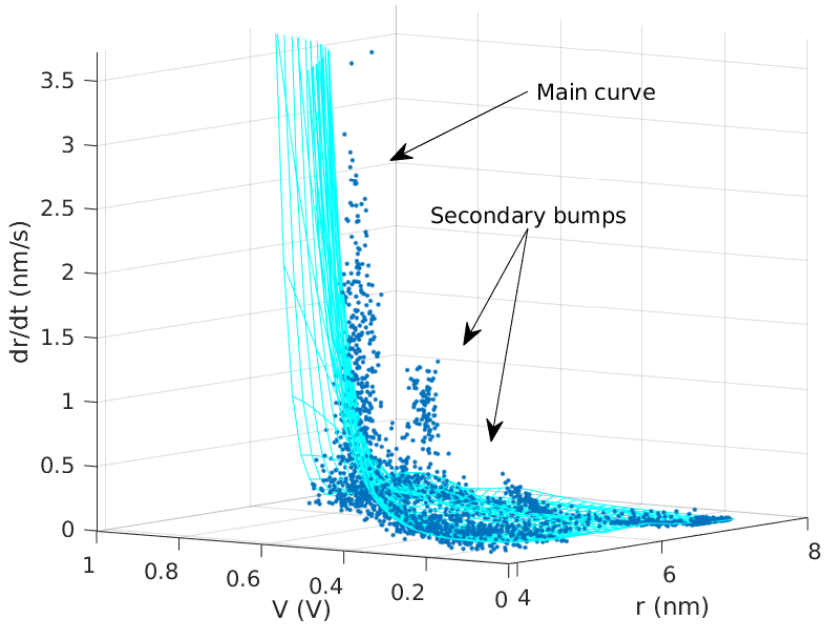

Figure 12: Rotation of the 3D plot of the experimental DRM, showing the presence of two secondary bumps on the main surface, caused probably by the existence of different CF. The points correspond to the whole range of extracted [V, r, dr/dt] triplets, and the grid corresponds to an empirical fit of those points.

5. Conclusion

In this paper we have made a presentation of the Dynamic Route Map (DRM) concept and its great potential in the modelling and analysis of memristive devices. To do so, we have tackled with the DRM analysis from the modelling side on a first step. In particular, we have addressed the issue by means of two memristor models based on different paradigms. The first of those models is based on a physical description of the memristor, assuming filamentary conduction. It is described by an explicit equation for the radius variation, that, under the convenient formulation, leads to the calculation of the system DRM. We have plotted this DRM, and we have shown that different effects (reset voltage dependence on the waveform, variation of the device behaviour caused by different waveforms, etc.) are easily explained using this framework. We followed the same approach using a second model, which is based on a memristor definition through a nonlinear analytical link between the device charge and flux. We have also derived an expression for the CF radius, and plotted the DRM for this second model, obtaining a shape that resembles the one of the previous case.

As a second complementary step, we have extracted experimentally the DRM of a ReRAM device. This is an interesting task, involving many modelling assumptions and measurement noise. We considered a truncated-cone shape for the conductive filament, and extracted the CF average radius in much the same way than for the charge-flux model. The results show that all the points

move very close to the surface generated by the DRM, independently of the input voltage signal waveform, or the actual considered cycle. Consequently, we have shown that, actually, the memristors are not behaving differently under different stimuli. It is simply that the observed device response is the projection on the I-V variables of a trajectory on a different phase space determined by a governing state variable, its rate of change, and the input stimulus. The relation between these magnitudes is what really defines the device behaviour, and, as shown, this relation can be experimentally determined.

Acknowledgment

We thank the Spanish Ministry of Science for Projects DPI2017-86610-P, TEC2017-84877-R, TEC2017-84321-C4-1-R, and TEC2017-84321-C4-3-R (also supported by the FEDER program). This work has made use of the Spanish ICTS Network MICRONANOFABS.

References

[1] L. O. Chua, "Memristor-the missing circuit element," *Circuit Theory, IEEE Transactions on*, vol. 18, no. 5, pp. 507–519, 1971.

[2] T. Prodromakis, C. Toumazou, and L. Chua, "Two centuries of memristors," *Nature materials*, vol. 11, no. 6, pp. 478–481, 2012.

[3] L. Chua and S. M. Kang, "Memristive devices and systems," *Proceedings of the IEEE*, vol. 64, no. 2, pp. 209–223, Feb 1976.

[4] R. Tetzlaff, *Memristors and memristive systems*. Springer, 2013.

[5] H. Kim, M. P. Sah, C. Yang, and L. O. Chua, "Memristor-based multilevel memory," in *Cellular nanoscale networks and their applications (CNNA), 2010 12th international workshop on*. IEEE, 2010, pp. 1–6.

[6] S. Stathopoulos, A. Khiat, M. Trapatseli, S. Cortese, A. Serb, I. Valov, and T. Prodromakis, "Multibit memory operation of metal-oxide bi-layer memristors," *Scientific reports*, vol. 7, no. 1, pp. 1–7, 2017.

[7] K. Eshraghian, K.-R. Cho, O. Kavehei, S.-K. Kang, D. Abbott, and S.-M. S. Kang, "Memristor mos content addressable memory (mcam): Hybrid architecture for future high performance search engines," *IEEE Transactions on Very Large Scale Integration (VLSI) Systems*, vol. 19, no. 8, pp. 1407–1417, 2011.

[8] S. Carrara, D. Sacchetto, M.-A. Doucey, C. Baj-Rossi, G. De Micheli, and Y. Leblebici, "Memristive-biosensors: A new detection method by using nanofabricated memristors," *Sensors and Actuators B: Chemical*, vol. 171, pp. 449–457, 2012.

[9] I. Gupta, A. Serb, A. Khiat, R. Zeitler, S. Vassanelli, and T. Prodromakis, "Memristive integrative sensors for neuronal activity," *arXiv preprint arXiv:1507.06832*, 2015.

[10] Y. V. Pershin and M. Di Ventra, "Experimental demonstration of associative memory with memristive neural networks," *Neural Networks*, vol. 23, no. 7, pp. 881–886, 2010.

[11] J. Grollier, D. Querlioz, and M. D. Stiles, "Spintronic nanodevices for bioinspired computing," *Proceedings of the IEEE*, vol. 104, no. 10, pp. 2024–2039, 2016.

[12] B. Sun, X. Zhang, G. Zhou, P. Li, Y. Zhang, H. Wang, Y. Xia, and Y. Zhao, "An organic nonvolatile resistive switching memory device fabricated with natural pectin from fruit peel," *Organic Electronics*, vol. 42, pp. 181–186, 2017.

[13] S. Battistoni, A. Dimonte, and V. Erokhin, "Organic memristor based elements for bio-inspired computing," in *Advances in Unconventional Computing*. Springer, 2017, pp. 469–496.

[14] D. B. Strukov, G. S. Snider, D. R. Stewart, and R. S. Williams, "The missing memristor found," *nature*, vol. 453, no. 7191, pp. 80–83, 2008.

[15] C. Dias, H. Lv, R. Picos, P. Aguiar, S. Cardoso, P. Freitas, and J. Ventura, "Bipolar resistive switching in Si/Ag nanostructures," *Applied Surface Science*, 2017.

[16] S. Brivio, G. Tallarida, E. Cianci, and S. Spiga, "Formation and disruption of conductive filaments in a HfO_2/tin structure," *Nanotechnology*, vol. 25, no. 38, p. 385705, 2014.

[17] B. Mohammad, M. A. Jaoude, V. Kumar, D. M. Al Homouz, H. A. Nahla, M. Al-Qutayri, and N. Christoforou, "State of the art of metal oxide memristor devices," *Nanotechnology Reviews*, vol. 5, no. 3, pp. 311–329, 2016.

[18] J. Kalomiros, S. G. Stavrinides, and F. Corinto, "A two-transistor non-ideal memristor emulator," in *Modern Circuits and Systems Technologies (MOCAST), 5th International Conference on*. IEEE, 2016, pp. 1–4.

[19] O. Camps, M. M. Al Chawa, C. de Benito, M. Roca, S. G. Stavrinides, R. Picos, and L. O. Chua, "A purely digital memristor emulator based on a flux-charge model," in *2018 25th IEEE International Conference on Electronics, Circuits and Systems (ICECS)*. IEEE, 2018, pp. 565–568.

[20] M. M. Al Chawa, C. de Benito, M. Roca, R. Picos, and S. Stavrinides, "Design and implementation of passive memristor emulators using a charge-flux approach," in *2018 IEEE International Symposium on Circuits and Systems (ISCAS)*. IEEE, 2018, pp. 1–5.

[21] O. Camps, R. Picos, C. de Benito, M. M. Al Chawa, and S. G. Stavrinides, "Emulating memristors in a digital environment using stochastic logic," in *2018 7th International Conference on Modern Circuits and Systems Technologies (MOCAST)*. IEEE, 2018, pp. 1–4.

[22] I. Messaris, A. Serb, A. Khiat, S. Nikolaidis, and T. Prodromakis, "A compact verilog-a ReRAM switching model," *arXiv preprint arXiv:1703.01167*, 2017.

[23] P. S. Georgiou, S. N. Yaliraki, E. M. Drakakis, and M. Barahona, "Window functions and sigmoidal behaviour of memristive systems," *International Journal of Circuit Theory and Applications*, 2016.

[24] A. Ascoli, R. Tetzlaff, and L. Chua, "Continuous and differentiable approximation of a TaO memristor model for robust numerical simulations," in *Emergent Complexity from Nonlinearity, in Physics, Engineering and the Life Sciences*. Springer, 2017, pp. 61–69.

[25] F. Jimenez-Molinos, M. Villena, J. Roldan, and A. Roldan, "A spice compact model for unipolar RRAM reset process analysis," *IEEE Transactions on Electron Devices*, 2015.

[26] Q. Li, A. Serb, T. Prodromakis, and H. Xu, "A memristor spice model accounting for synaptic activity dependence," *PloS one*, vol. 10, no. 3, p. e0120506, 2015.

[27] J. Secco, F. Corinto, and A. Sebastian, "Flux-charge memristor model for phase change memory," *IEEE Transactions on Circuits and Systems II: Express Briefs*, 2017, in press.

[28] R. Picos, J. B. Roldan, M. M. Al Chawa, P. Garcia-Fernandez, F. Jimenez-Molinos, and E. Garcia-Moreno, "Semiempirical modeling of reset transitions in unipolar resistive-switching based memristors," *RADIOENGINEERING*, vol. 24, no. 2, p. 421, 2015.

[29] E. Garcia-Moreno, R. Picos, and M. M. Al-Chawa, "Spice model for unipolar RRAM based on a flux-controlled memristor," in *Power, Electronics and Computing (ROPEC), 2015 IEEE International Autumn Meeting on*. IEEE, 2015, pp. 1–4.

[30] M. M. Al Chawa, R. Picos, J. B. Roldan, F. Jimenez-Molinos, M. A. Villena, and C. de Benito, "Exploring resistive switching-based memristors in the charge–flux domain: a modeling approach," *International Journal of Circuit Theory and Applications*, pp. n/a–n/a, 2018, cta.2397. [Online]. Available: http://dx.doi.org/10.1002/cta.2397

[31] Z. Kolka, D. Biolek, V. Biolkova, and Z. Biolek, "Evaluation of memristor models for large crossbar structures," in *Radioelektronika (RADIOELEKTRONIKA), 2016 26th International Conference*. IEEE, 2016, pp. 91–94.

[32] R. Picos, J. Roldan, M. Al Chawa, F. Jimenez-Molinos, and E. Garcia-Moreno, "A physically based circuit model to account for variability in memristors with resistive switching operation," in *Design of Circuits and Integrated Systems (DCIS), Conference on*. IEEE, 2016, pp. 1–6.

[33] R. Naous, M. Al-Shedivat, and K. N. Salama, "Stochasticity modeling in memristors," *IEEE Transactions on Nanotechnology*, vol. 15, no. 1, pp. 15–28, 2016.

[34] F. Corinto, P. P. Civalleri, and L. O. Chua, "A theoretical approach to memristor devices," *IEEE Journal on Emerging and Selected Topics in Circuits and Systems*, vol. 5, no. 2, pp. 123–132, 2015.

[35] L. O. Chua, "Everything you wish to know about memristors but are afraid to ask," *Radioengineering*, vol. 24, no. 2, p. 319, 2015.

[36] S. Shin, K. Kim, and S.-M. Kang, "Compact models for memristors based on charge-flux constitutive relationships," *Computer-Aided Design of Integrated Circuits and Systems, IEEE Transactions on*, vol. 29, no. 4, pp. 590–598, 2010.

[37] R. Picos, M. M. Al Chawa, M. Roca, and E. Garcia-Moreno, "A charge-dependent mobility memristor model," in *Proceedings of the 10th Spanish Conference on Electron Devices, CDE'2015*. IEEE, 2015.

[38] R. Picos, J. B. Roldan, M. M. Al Chawa, F. Jimenez-Molinos, M. Villena, and E. Garcia-Moreno, "Exploring ReRAM-based memristors in the charge-flux domain, a modeling approach," in *Proceedings of International Conference on Memristive Systems, MEMRISYS'2015*, 2015.

[39] C. de Benito, M. M. Al Chawa, R. Picos, and E. Garcia-Moreno, "A procedure to calculate a delay model for memristive switches," in *Workshop on Memristor Technology, Design, Automation and Computing*, 2017.

[40] A. Theodorakakos, S. G. Stavrinides, E. Hatzikraniotis, and R. Picos, "A non-ideal memristor device," in *Memristive Systems (MEMRISYS) 2015 International Conference on*. IEEE, 2015, pp. 1–2.

[41] M. M. Al Chawa, A. Rodriguez-Fernandez, M. Bargallo, F. Campabadal, C. de Benito, S. Stavrinides, E. Garcia-Moreno, and R. Picos, "Waveform and frequency effects on reset transition in bipolar ReRAM in flux-charge space," in *Memristive Systems (MEMRISYS) 2017 International Conference on*. IEEE, 2017.

[42] M. M. Al Chawa, R. Picos, E. Covi, S. Brivio, E. Garcia-Moreno, and S. Spiga, "Flux-charge characterizing of reset transition in bipolar resistive-switching memristive devices," in *11th Spanish Conference on Electron Devices*, 2017.

[43] J. Liouville, "Sur la théorie de la variation des constantes arbitraires," *Journal des Mathématiques Pures et Applications*, vol. 3, pp. 342–349, 1838.

[44] H. Poincaré, "Les méthodes nouvelles de la mécanique céleste," vol. 3, 1892-99.

[45] P. Ehrenfest and T. Ehrenfest, "Encyklopadie der mathematischen wissenschaften," vol. 4, 1911.

[46] L. O. Chua, "If it's pinched it's a memristor," *Semiconductor Science and Technology*, vol. 29, no. 10, p. 104001, 2014.

[47] ——, "Five non-volatile memristor enigmas solved," *Applied Physics A*, vol. 124, no. 8, p. 563, 2018.

[48] D. Ielmini, F. Nardi, and C. Cagli, "Physical models of size-dependent nanofilament formation and rupture in NiO resistive switching memories," *Nanotechnology*, vol. 22, no. 25, p. 254022, 2011.

[49] A. Rodriguez-Fernandez, J. Suñé, E. Miranda, M. B. Gonzalez, F. Campabadal, M. M. Al Chawa, and R. Picos, "Spice model for the ramp rate effect in the reset characteristic of memristive devices," in *2017 32nd Conference on Design of Circuits and Integrated Systems (DCIS)*, 2017, pp. 1–4.

[50] M. M. Al Chawa, C. de Benito, and R. Picos, "A simple piecewise model of reset/set transitions in bipolar ReRAM memristive devices," *IEEE Transactions on Circuits and Systems I: Regular Papers*, vol. 65, no. 10, pp. 3469–3480, Oct 2018.

[51] M. M. Al Chawa and R. Picos, "A simple quasi-static compact model of bipolar ReRAM memristive devices," *IEEE Transactions on Circuits and Systems II: Express Briefs*, vol. 67, no. 2, pp. 390–394, 2020.

[52] M. M. Al Chawa, R. Picos, and R. Tetzlaff, "A simple memristor model for neuromorphic ReRAM devices," in *Circuits and Systems (ISCAS), 2020 IEEE International Symposium on."Accepted".* IEEE, 2020.

[53] M. M. Al Chawa, S. G. Stavrinides, C. de Benito, M. Bargallo, and R. Picos, "A non-quasi static model for reset voltage variation in memristive devices," in *2019 26th IEEE International Conference on Electronics, Circuits and Systems (ICECS)*, 2019, pp. 1–4.